Prebreakdown energy absorption from intense laser pulses at 532 nm in NaCl

Scott C. Jones, Alfred H. Fischer,* and Peter Braunlich
Department of Physics, Washington State University, Pullman, Washington 99164-2814

Paul Kelly
National Research Council, Ottawa, Canada K1A 0R6
(Received 10 June 1987)

Details of the photoacoustic measurement and model calculations of prebreakdown energy deposition in NaCl at 532 nm [Jones, Shen, Braunlich, Kelly, and Epifanov, Phys. Rev. B **35**, 894 (1987)] are provided. The primary absorption process is shown to be four-photon excitation of valence electrons to the conduction band. Calibration of the acoustic system by two-photon absorption of 266-nm laser light indicates focal point temperature increases over 300 K are attained for nondamaging pulses at 532 nm. Interpretation of the experimental data considering secondary energy absorption by free carriers and transient crystal defects yields the result that the generalized four-photon cross section lies in the range 1×10^{-114} cm^8 sec^3 $\leq\sigma^{(4)}\leq 20\times10^{-114}$ cm^8 sec^3. It is further shown that avalanche generation of free carriers is not evident even for these large temperature increases. The calibrated results were obtained from reactive-atmosphere-processed ultrapure NaCl crystals; the importance of sample purity is discussed.

I. INTRODUCTION

A nominally transparent, wide-band-gap solid may be rendered an absorber when exposed to laser light of sufficiently high intensity. Interest in this phenomenon is usually related to laser-induced damage of optical components. The mechanism(s) of induced absorption and damage are generally held to depend on the relative sizes of the laser photon energy, $h\nu$, and the material band gap, E_g. For $h\nu/E_g \ll 1$, laser damage is attributed to avalanche ionization and subsequent Joule heating of the lattice through interaction of free carriers with the strong electric field of the laser pulse.[1] When the photon energy is a significant fraction of the band gap, however, multiphoton absorption by valence-band electrons may either contribute to or be the dominant mechanism of free-carrier production. The probability of simultaneous absorption of m photons, where $m \geq E_g/h\nu \geq m-1$, drops precipitously with increasing order m. For which order multiphoton absorption becomes important to laser damage is not precisely known. Deficiencies in the avalanche theory led Braunlich *et al.* to propose that multiphoton absorption contributes to or is primarily responsible for damage in alkali halides for cases where the band gap is bridged by 3, 4, or 5 photons ($m=3-5$).[2-4] While the frequency and pulse width dependence of the damage threshold (the maximum intensity or electric field strength of a laser pulse that just causes—subjectively defined—damage) in alkali halides appears to be consistent with the avalanche model for $m \geq 5$, insufficient and contradictory data exist for $m=4$ in NaCl ($E_g=8.6$ eV, $h\nu=2.33$ eV) to unequivocally assign damage to the avalanche mechanism.[1,5,6] Thus it is important to measure energy absorption prior to damage to determine which mechanism is operative in this case. Attainment of this goal requires use of a technique highly sensitive to small absorbed energies arising from high-energy pulses. A simple direct attenuation experiment is inadequate for high-order absorption processes.

Theoretical modeling of laser-induced damage has been hampered by a lack of reliable or accurate values for critical parameters, e.g., multiphoton absorption cross sections and electron-phonon scattering frequencies. Experimental evidence supporting theories of laser damage has hitherto centered on the laser frequency and pulse width dependence of the damage threshold. The purpose of this paper is to report the details of a successful measurement of calibrated prebreakdown energy deposition in NaCl exposed to intense pulses of 532-nm laser light using the photoacoustic technique.[7] The primary process is shown to be valence electron excitation via four-photon absorption. The calibrated data also allow analysis of secondary absorption processes as well as calculation of the temperature increase at the geometrical focus of a beam tightly focused in the bulk of the single crystal samples. Large temperature increases (>300 K) are obtained without evidence of electron avalanche formation.

Demonstration of the nonlinear order of the excitation, i.e., the number of photons absorbed by valence electrons in the primary excitation process, is given by the dependence of the signal on the incident laser pulse energy.[8] The photoacoustic technique yields a response proportional to the absorbed energy. While it demonstrates the occurrence of four-photon absorption, it also responds to energy absorbed in secondary processes, e.g., conduction-band carrier and primary lattice defect absorption, and thus one cannot arrive at an unambiguous value for the four-photon cross section without careful analysis of these secondary absorption processes.

An extensive review of theoretical and experimental results pertaining to multiphoton absorption in crystalline solids was recently performed by Nathan *et al.*[9]

The free-carrier generation rate can be written as

$$dn_c/dt = N\sigma^{(m)}F^m , \quad (1)$$

where $\sigma^{(m)}$ is the generalized m-photon absorption cross section, F is the photon flux, and N is the density of absorbing species. In NaCl, N represents the density of Cl^- ions in the crystal. Four- and five-photon absorption have previously been observed in alkali halides,[10,11] and Catalano *et al.*[12] have reported four-photon absorption cross sections in KBr and KI and five-photon cross sections in KCl and NaCl, obtained by the photoconductivity method under ruby illumination. However, these measurements have been severely criticized and deemed invalid by Williams *et al.*,[13] who showed that crucial assumptions made by Catalano *et al.* regarding the free-carrier lifetimes were incorrect. A recent determination of $\sigma^{(4)}$ in KBr using the self-trapped exciton recombination luminescence technique, which is more reliable than the photoconductivity method, yielded $\sigma^{(4)}=(2\pm1)\times10^{-112}$ cm^{8}sec^3 at 532 nm.[14] The lack of a reliable value for $\sigma^{(4)}$ in NaCl was the prime motivation for this project.

The rest of this paper is divided into four major sections. In Sec. II we discuss the photoacoustic technique for measuring energy absorption. Section III is concerned with experimental details, calibrated absorption measurements, and indicated upper limits for $\sigma^{(4)}$. In Sec. IV calculations modeling the overall crystal-pulse interaction are presented and avalanche ionization is also considered. Section V is comprised of the summary and conclusions.

II. PHOTOACOUSTIC TECHNIQUE FOR MEASUREING ABSORBED ENERGY

Previous photoacoustic measurements of nonlinear absorption include those by Tam and Patel[15] in benzene, and two-photon absorption in solids by Van Stryland and Woodall,[16] Munir *et al.*,[17] Bae *et al.*,[18,19] and Gorshkov *et al.*[20] Three-photon absorption was detected by Van Stryland *et al.*,[21] and Horn *et al.*[22,23] reported a calibrated measurement of energy deposition by three-photon absorption in a solid.

The bulk of the literature on the photoacoustic detection of optical absorption has focused on weak linear absorption of unfocused laser beams in liquids. The technique in this regard has been thoroughly reviewed,[24,25] but the theoretical aspects in crystalline solids have been only sparsely investigated. However, for the technique to be useful for measuring absolute energy deposition, we require only that a calibration be obtainable and that the calibration conditions hold in the case of measuring the unknown absorption. We use the second and fourth harmonics of Nd:YAG (where YAG denotes yttrium aluminum garnet) in the present experiments. The absorption of four 532-nm photons and two 266-nm photons results in the same absorbed energy in the primary multiphoton process. Two-photon absorption, however, is easily measured by attenuation. Therefore, after four-photon absorption is established, the system is calibrated by measuring the attenuation of 266-nm pulses under focal conditions which are carried over to the four-photon case at 532 nm.

The thermal acoustic source generated by the nonlinear absorption of a tightly focused laser pulse in a nominally transparent material is much more localized than the usual (unfocused or cylindrical) source considered in photoacoustic theory. The laser pulse is focused to a radius w_0 of 10 μm or less, near the midplane of a slab of single crystal NaCl of approximate dimensions $5\times10\times30$ mm^3, with the entrance and exit faces being the 5×30 surfaces. The focal point is on the plane bisecting the 5×30 surface at the midpoint of the beam path through the crystal. The crystal is bonded to a fused silica plate, of truncated elliptical shape, on which a lead zirconate titanate (PZT) transducer is affixed (Fig. 1).[22,23] The separation of sample and transducer allows discrimination of scattered light from signal[26] and the elliptical shape provides some focusing of acoustic waves on the transducer.[27] This complicated arrangement makes impractical solving for the pressure wave at the transducer. However, it is sufficient to show that one can have equivalent acoustic sources under 266- and 532-nm illumination, making the boundary conditions and wave form irrelevant, and that a valid calibration can be obtained. In this regard, we ignore the crystalline nature of the sample and assume it to be isotropic and consider generation of longitudinal waves only. Liu[28] has shown that a temperature field (thermal source) cannot generate transverse waves in an isotropic solid. Thus the problem reduces to that of solving for

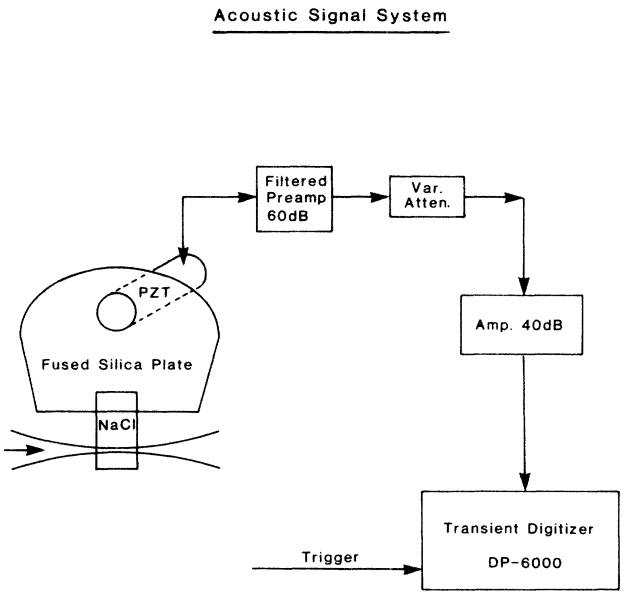

FIG. 1. Schematic diagram of the acoustic signal detection apparatus. The laser pulse traverses the sample in the direction shown, with focal point on midplane of NaCl crystal. The PZT transducer has resonant frequency of 175 kHz, matched with a narrow band-pass filter in the 60 dB preamplifier. The signal passes through a variable attenuator and then is amplified by 40 dB fixed gain final amplifier before measurement with a transient digitizer.

the pressure wave in an infinite "fluid" for a given source.

In Ref. 29 we present a detailed derivation of the pressure wave induced by the nonlinear absorption of a single sharply focused laser pulse as sensed by an acoustic transducer of resonant angular frequency ω. A multipole expansion of the Green's function is carried out for generalized source terms in an unbounded fluid, and an integration over the nonlinear interaction volume is performed for both thermal and electrostrictive sources. Under the focal conditions for Gaussian beams the intensity is

$$I(\mathbf{r},t)=\frac{E(1-R)\exp[-r^2/w_0^2(1+z^2/z_0^2)]}{\pi^{3/2}w_0^2\tau(1+z^2/z_0^2)} \times \exp(-t^2/\tau^2) , \quad (2)$$

where the photon flux is $F=I/h\nu$, r the radius in cylindrical coordinates from the pulse propagation axis, z the distance from the focal plane along the axis, w_0 the $1/e$ intensity radius on the focal plane, z_0 the confocal parameter ($z_0=2\pi w_0^2 n/\lambda$), E the pulse energy, τ the pulse halfwidth at $1/e$ intensity, and R is the reflectivity of the crystal entrance face.

Considering now energy deposition due to multiphoton absorption only, and assuming instantaneous recombination, the rate of energy absorption per unit volume, and temperature rise, will be given by

$$\partial u(\mathbf{r},t)/\partial t=4h\nu\sigma^{(4)}N[F(\mathbf{r},t)]^4 ,$$

and

$$\rho c\,\partial T(\mathbf{r},t)/\partial t=\partial u(\mathbf{r},t)/\partial t , \quad (3)$$

respectively, where ρ is the mass density and c the specific heat at constant pressure. The total absorbed energy is $U=\int d^3r\,dt\,\partial u(\mathbf{r},t)/\partial t$. If we introduce the interaction volume

$$V=\int d^3r\left[\frac{\exp[-r^2/w_0^2(1+z^2/z_0^2)]}{1+z^2/z_0^2}\right]^4 \approx 3\pi^2 w_0^2 z_0/32, \quad \text{if } z_0/d<\tfrac{1}{5} , \quad (4)$$

where d is the crystal thickness, then

$$U=2\sqrt{\pi}h\nu\sigma^{(4)}N\tau[E(1-R)/\pi^{3/2}w_0^2\tau h\nu]^4V . \quad (5)$$

The integrand in Eq. (4) is the spatial distribution function of the absorbed energy and, thus, the temperature, immediately after the laser pulse has passed through the interaction volume, i.e., before diffusion, which is slow compared to $\tau<10^{-10}$ sec, has progressed to any extent. The diffusion time is approximately $\rho c w_0^2/k\approx 5\times10^{-6}$ sec for NaCl and $w_0\approx 5$ μm, thermal conductivity, $k=0.092$ W/deg cm, $\rho=2.165$ g/cm^3 and $c=0.864$ J/g deg. The maximum temperature increase is at the origin ($\mathbf{r}=0$) and is

$$\Delta T_0=U/\rho cV=(16\lambda/3\pi^3\rho c w_0^4 n)U . \quad (6)$$

Solving Eqs. (4) and (5) for the cross section we obtain

$$\sigma^{(4)}=\frac{8\pi^3 w_0^4\tau^3(h\nu)^3\lambda}{3\sqrt{\pi}Nn[(1-R)E]^4}U . \quad (7)$$

The symmetry of the generalized source for m-photon absorption, $u(\mathbf{r})$, causes the dipole moment of the acoustic source to vanish, leaving monopole and quadrupole terms.[29]

The monopole term of the pressure is

$$p_m(\mathbf{r},\omega)\cong -i\omega\beta\exp(i\omega r/v_s) \times \exp[-(\omega^2\tau^2/4m)]U_m/(4\pi cr) ,$$

where β is the thermal expansion coefficient and v_s is the longitudinal sound speed. Therefore, to lowest order, the acoustic signal is proportional to the energy, U_m, absorbed by m-photon excitation.

For beam propagation along the z axis, the xx and yy quadrupole components are entirely negligible under any conditions of sample size, but care must be exercised with the zz component in a bounded medium. However, we have shown that calibration error arising from the disagreement between the zz quadrupole components for the 532- and 266-nm pulses is 10% or less.[29]

Considering acoustic generation by electrostriction[30] led us to conclude that, for isotropic condensed matter, or circularly polarized light in a crystalline solid, the monopole and dipole terms vanish, and the remaining quadrupole contributions result in an electrostrictive source strength of the order 10^{-8} of the thermal monopole source. We then assumed that linear polarized light in a crystalline solid would yield similarly negligible contributions.

Therefore, the calibration consists merely of determining the acoustic signal generated by energy deposition via two-photon absorption under focal conditions in which the quadrupole source terms are negligible in comparison with the dominant monopole term, and the centers of the monopoles for both the two- and four-photon absorption measurements coincide. The energy deposited by four-photon absorption is then calculated from the signal generated under 532-nm illumination.

The value of ΔT_0 is obtained under the assumption of negligible diffusion of both heat and free carriers, and beam deformation is disregarded. The first condition is easily satisfied under the focal conditions and time scales of the experiments; carrier diffusion and beam deformation are discussed below. We note that the deposited energy measurements are valid regardless of the absorption mechanism, and that the temperature calculation is valid if four-photon absorption is the primary deposition mechanism, as demonstrated by the dependence of the acoustic signal on the incident pulse energy.

For the acoustic signal, S, proportional to the pressure, we see that the slope on a double-logarithmic plot, $\partial(\log S)/\partial(\log E)$, of approximately four (depending on signal-to-noise ratio) is expected for four-photon absorption. A measured slope of four is taken as verification that a four-photon absorption process is occurring and the calibration procedure is valid.

III. EXPERIMENTAL DETAILS

A. Apparatus

The laser system has been described elsewhere.[14] A variety of fused silica lenses were used in our experiments, the selection of any one being dictated by the size of interaction volume desired. They were all of the plano-convex or "best form" type. Measurement of beam profiles is carried out at the lens input plane by a scanning slit method. The slit width, s, is smaller than the scan displacement increment, Δx, which in turn is approximately 1% of the beam diameter. The slit is driven by a computer controlled, high resolution stepper motor, and the slit throughput is normalized with respect to incident pulse energy on a shot by shot basis. The slit is displaced a distance Δx between each laser pulse, and several scans are performed to check consistency. Scanning may be done in any direction in the plane normal to the beam axis.

A spatially Gaussian beam with infinite wave front radius of curvature (no divergence) and intensity profile $I_{\text{in}}=I_0\exp(-r^2/\rho^2)$ incident paraxially on the input plane of the lens, will have diffraction limited intensity distribution on the output side of the lens given by Eq. (2).[31] Detailed calculations on the Gaussian beam using matrix optics techniques[31] show that, in the diffraction limit, when the sample surface is between the lens and the focal point, the spot radius does not change, but the focal point is shifted by a small distance related to the crystal refractive index, n. Therefore, $z_0=2\pi w_0^2 n/\lambda$ is the correct confocal parameter in the crystal. The location of the focal point in the crystal is easily found (for short focal length) by irradiating the sample with a damaging laser pulse.

Spherical aberration effects on the spot size w_0 have been analyzed in detail.[32] For the large effective f/numbers used in our experiments ($f/2\rho>20$), spherical aberration is entirely negligible. We henceforth assume diffraction limited performance and determine the Gaussian beam parameter w_0 by scanning the lens input to obtain ρ and use the relation $w_0=f\lambda/2\pi\rho$. The input beam was checked for collimation and no discernible divergence was found within the error of the apparatus ($\pm 5\%$). The effect of self-focusing on spot size will be discussed after the data are presented.

A schematic of the acoustic system is shown in Fig. 1. The transducer is an Acoustic Emission Technology model AC-175L resonant PZT transducer, differentially coupled to a 60 dB preamp which contains a narrow band filter matched to the 175 kHz resonant frequency of the transducer. The high-resonant frequency makes the system immune to ambient laboratory noise. The acoustic signals are fed to a Data Precision 6000 transient digitizer (TD). The limited resolution and input range of the TD creates a need for more amplification and/or attenuation of the preamp output. A calibrated, variable coaxial attenuator (DC-4 GHz bandwidth) is inserted between the preamp and fixed gain (40 dB) final amplifier, in order to maintain the signal fed to the TD at a level such that the relative accuracy is reasonable compared with the absolute uncertainty (10 mV) of the signal level. The TD was also used to simultaneously monitor pulse energies.

The laser pulse traverses the crystal with the orientation shown in Fig. 1. With a typical confocal parameter $z_0\approx 1$ mm and path length $d\approx 10$ mm, the peak intensity on the crystal surface will be down by a factor $(1+z^2/z_0^2)=26$ from that at the focal point. This is a very important aspect of the experiment for two reasons. First, the surface damage threshold intensity is generally much smaller than that of the bulk because of impurities and surface roughness. Second, a low intensity will reduce the signal generated by nonlinear surface interactions, and we can be certain that only bulk phenomena are observed.

The acoustic signal consists of a modulated sine wave; we use the peak-to-peak amplitude as the measure for the absorbed energy.

B. Experimental procedure

1. Preliminary experiments and samples

Demonstrating the occurrence of four-photon absorption in solids, though a simple matter in principle, is not trivial and requires careful choice of experimental conditions. By and large, the main difficulty we encountered was in obtaining a set of data points before the crystal was damaged. Out of a collection of some 15 samples of laser grade NaCl from Harshaw Chemical Co., and seven samples cut from a single boule of ultrapure NaCl obtained from the Crystal Growth Laboratory at the University of Utah, only two yielded prebreakdown signals attributable to four-photon absorption.

An observation of the damage threshold distribution in a collection of NaCl crystals was reported by Manenkov[33] (also see Ref. 5). In over 100 different crystals tested for damage threshold under identical spatio-temporal pulse energy conditions, an approximately normal distribution about a mean threshold was measured together with a tight group of results with values about four times the mean. These latter thresholds were interpreted as intrinsic damage events. This led us to try to obtain crystals of higher purity, in order to increase the probability of having samples of sufficiently high damage threshold to yield prebreakdown acoustic signals.

We found that ultrapure reactive-atmosphere processed NaCl crystals (obtained from the Crystal growth Laboratory at the University of Utah) had sufficiently high damage thresholds for consistent measurements of prebreakdown energy deposition. This material contains alkali and alkaline earth impurities (notably K, Li, Ba, Rb, Sr, and Mg) at a 0.1 to 5 ppm (parts per million) level together with other metallic impurities (Al, Fe, Cu, Ni, Tl, and Zn) at less than 0.01 ppm.[34] Processing the starting material in an HCl atmosphere reduces the normally present OH^- concentrations of a few ppm by 1 or 2 orders of magnitude. With these crystals, we obtained fourth-order power-law dependence of acoustic signal on incident energy (slope of a double-logarithmic plot of signal versus incident pulse energy) over a dozen times

in samples with damage thresholds ranging from 400 to over 500 GW/cm^2. Crystals with higher thresholds yielded slopes nearer to four; the range was from 3.55 ± 0.15 to 3.95 ± 0.4.[29] We thus did not pursue the purity issue any further.

The presence of OH^- has some implications for acoustic signal versus absorbed energy calibrations.[35,36] First, buildup of F centers due to x-ray exposure (producing electron-hole pairs) is initially proportional to OH^- concentration, implying that multiple laser shots on one site could lead to efficient production of stable defects in the interaction volume. Secondly, an OH^- associated emission of yellow-green fluorescence peaks with excitation at 260 nm. Thus OH^- contaminated NaCl will be a linear absorber of the calibration light source, leading to error in the calibration.[37] In Ref. 35 it is also noted that the OH^- concentration of thin sections varies according to the position in the boule from where it came.

2. *Calibration of deposited energy versus incident pulse energy*

Measurements of the energy deposited in the crystal due to absorption of 532-nm photons requires calibration of the acoustic system with a known absorbed energy, provided by 266-nm photons in our case. The following steps are involved.

(1) The 532- and 266-nm beam profiles are obtained using the scanning apparatus. After beam scanning, the focusing lens is installed and aligned.

(2) By varying laser pulse energy, we obtain acoustic signal versus incident energy. If sufficient prebreakdown data indicating four-photon absorption are obtained, we calibrate the incident pulse energy as measured by photodiodes from a pick-off beam splitter, using a calibrated energy meter at the sample position.

Step (2) provides the acoustic signal versus incident energy for 532-nm laser pulses. Calibration of the acoustic detector is carried out by measuring the acoustic signal simultaneously with the energy of single 266-nm pulses absorbed by the crystal. Absorption of 266-nm light is a two-photon process in NaCl (for excitation of valence electrons across the gap), which allows us to approximate the acoustic emission volume as a monopole source.

(3) With 266-nm beam profile adjusted during step (1) for approximately equal interaction volumes (monopole moments), the pulse energy is varied to cover the range of acoustic signal obtained with 532-nm pulses, while simultaneously measuring the incident and transmitted energy. The uv calibration was checked for nonlinearity (two-photon attenuation corrected for reflectivity) by plotting acoustic signal versus incident energy on a double-logarithmic scale.

(4) The final step is to measure the 532-nm pulse temporal profile to obtain the pulse parameter τ, using the zero-background, second harmonic generation autocorrelation technique.[38,39] This task is performed last as it requires some rearrangement of optical components.

Although the detailed interaction of the crystal with 532-nm and 266-nm photons differs, the acoustic signal generated depends only on the conversion of excitations to thermal energy in the interaction volume. At room temperature and above radiative processes are quenched (see Sec. IV) and, thus, all excitations decay nonradiatively, resulting for the most part in heating of the interaction volume. As such, the calibration of the acoustic system using pulses of 266-nm light is a valid procedure.

We can determine $\sigma^{(4)}$ on a single shot basis with the acoustic calibration $S(U)$ and the incident energy E, by inverting $S(U)$ to obtain the absorbed energy from the acoustic signal, $U(S)$; or for a series of shots of varying incident energy.

If $S(U)=aU+b$, then $U=(S-b)/a$ and Eq. (7) becomes

$$\sigma^{(4)}=\frac{8\pi^3 w_0^4 \tau^3 (h\nu)^3 \lambda}{3\sqrt{\pi} N n (1-R)^4}\frac{(S-b)}{aE^4} . \tag{8}$$

Alternatively, we can fit the data points $[U(S),E]$ to

$$U = A\sigma^{(4)}E^4+\text{const} \tag{9}$$

with $A=3\sqrt{\pi}Nn(1-R)^4/8\pi^3 w_0^4\tau^3(h\nu)^3\lambda$.

The calibration procedure was carried out on three different samples of reactive atmosphere processed ultrapure NaCl, two cut from one boule, the third from a second boule. In all cases, the polarization of the incident 532-nm laser pulse was parallel to the [110] crystal direction with propagation along the [100] axis.

C. Results

1. *Crystal no. 1*

The first calibration was performed on a 4-mm thick wafer cut from the middle of the first boule. This sample was chosen purposely to see if a wafer from the middle of the boule was clean enough to yield prebreakdown data. That the crystal quality is critical is indicated by our observation that a sample from near the bottom of the boule did not yield a signal attributable to four-photon absorption before damage.

The data for this calibration are the lower set of eight in Fig. 2. The upper limit of the four-photon absorption cross section obtained from the data set is $\sigma^{(4)}_{\max}=(5.7\pm2.5)\times10^{-113}$ cm^{8}sec^3, calculated with Eq. (9). The relevant parameters are listed in Table I, as is the peak intensity of the highest predamage pulse.

This set of eight points was obtained on a single site in the crystal. The number was limited to avoid possible buildup of lattice defects (F centers) which are created as a result of electron-hole pair generation. The set was terminated when damage was detected, with points attributed to damage not included. Our damage criteria are (a) scattering of laser light at approximately 90° to the optic axis from the focal region coupled with (b) a

TABLE I. Parameters of energy deposition calibration and results. f, lens focal length; w_0, spot radius ($1/e$ intensity); τ, pulse temporal parameter; V, interaction volume; d, path length; I_{max}, maximum peak intensity of nondamaging pulse in data set; $\sigma^{(4)}_{max}$, upper limit of four-photon absorption cross section obtained from this data set. The 266-nm interaction volume V is given by $V=2\pi^2 w_0^4 n \tan^{-1}(d/2z_0)/\lambda$, where n, w_0, z_0, and λ refer to that appropriate for the uv wavelength.

Sample	f (mm)	w_0 (cm)	τ (psec)	V (cm^3) 532 nm	V (cm^3) 266 nm	d (cm)	I_{max} (GW/cm^2)	$\sigma^{(4)}_{max}$ (cm^8 sec^3)
1	66.7	6.32×10^{-4}	81	2.7×10^{-8}	2.6×10^{-8}	1	335	$(5.7\pm2.5)\times10^{-113}$
2	42.3	3.9×10^{-4}	86.7	4.0×10^{-9}	4.8×10^{-9}	0.46	590	$(4.3\pm2.4)\times10^{-113}$
3	66.7	8.4×10^{-4}	83	8.4×10^{-8}	9.7×10^{-8}	1	182	$(2.75\pm1)\times10^{-112}$

very large acoustic signal inconsistent with that generated by a pulse of similar energy before damage. The simultaneous observation of (a) and (b) signaled bulk damage. A further qualitatitive check is distortion of the transmitted beam profile, usually similar to a pinhole diffraction pattern, when the interaction volume is damaged. Damage at this level is not detected by visual inspection, in contrast to the visible damage track or filament usually taken as indication of catastrophic damage in most breakdown threshold measurements.[1,32]

Subsequent experiments with a longer focal length lens, performed in order to obtain data with lower peak intensities, led to surface damage and rendered this sample useless for further experimentation.

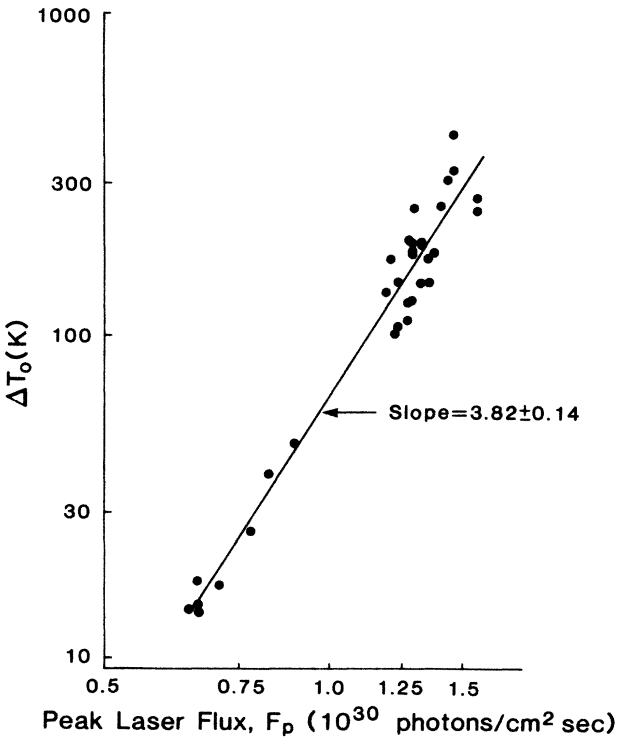

FIG. 2. Composite double-logarithmic plot of calculated temperature increase at focal point vs incident energy of 532-nm pulses for sample nos. 1 and 2. Sample no. 1 data (lower eight points) indicate an upper limit on $\sigma^{(4)}$ of $(5.7\pm2.5)\times10^{-113}$ cm^8 sec^3. The upper set of points, obtained from sample no. 2, yields an upper limit of $\sigma^{(4)}=(4.3\pm2.4)\times10^{-113}$ cm^8 sec^3.

2. *Crystal no. 2*

This sample was the second wafer from the top of the first boule (the very top wafer is unsuitable due to the growth characteristics). With this sample we tried a shorter focal length lens to obtain data at a higher peak intensity, since the damage threshold is expected to increase for smaller focal volumes. These data are the higher set of points in Fig. 2. We present them together with those from sample no. 1 as a composite plot in order to show the consistency for two different samples from the same boule, even under different focal conditions. The slope of the line in the double-logarithmic plot is 3.82 ± 0.14.

The data are a collection of 27 shots over eights sites in a small matrix (approximately 3 mm$\times$3 mm). The high intensities necessary to obtain signal (the apparatus is sensitive to absorbed energy, and we have a very small interaction volume in this data set) required this strategy. Pulses obviously producing damage were deleted from the data set.

The upper limit of $\sigma^{(4)}_{max}=4.3\times10^{-113}$ cm^8 sec^3, satisfactorily consistent with the result from sample no. 1, is the mean value of $\sigma^{(4)}$ calculated using Eq. (8) for the 27 points. The standard error of the mean is 0.25×10^{-113} cm^8 sec^3.

There is one point in this data set for which we are confident that we have measured a very high-temperature rise without damaging the crystal. This point is $\Delta T_0=324$ °C at $I_{peak}=550$ GW/cm^2. Subsequent pulses of lower intensity on this site were entirely consistent with the data set and exhibited no evidence of damage.

3. *Crystal no. 3*

The third sample is the second wafer from the top of the second boule. The data are presented in Fig. 3. They occur for lower intensities than for sample nos. 1 and 2, and we have a smaller slope of approximately 3.3 on the double-logarithmic plot. The pulse of highest energy without damaging the crystal had peak intensity of only 182 GW/cm^2. The slope is perhaps indicative of the presence of a lower-order process. We include the value of $\sigma^{(4)}_{max}$ obtained from these data to demonstrate the variation of results one might expect from using a variety of crystals. The upper limit for the four-photon absorption cross section obtained from these data, calculated with Eq. (9), is $\sigma^{(4)}_{max}=(2.75\pm1.0)\times10^{-112}$ cm^8 sec.[3]

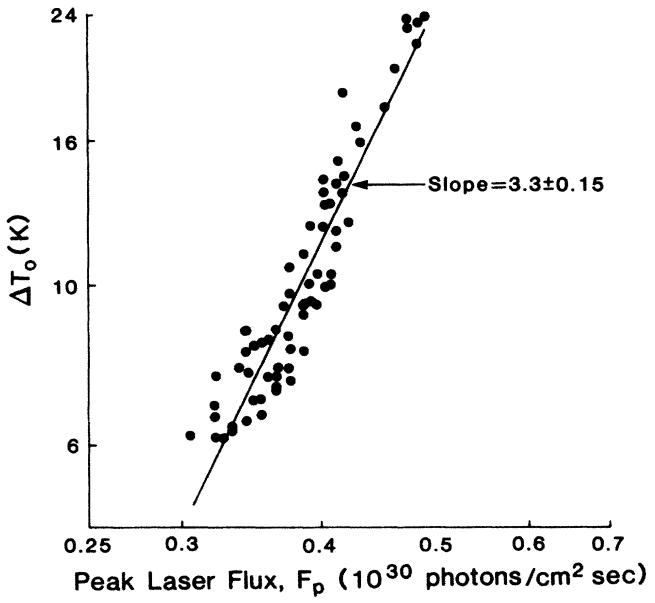

FIG. 3. Double-logarithmic plot of calculated temperature increase at focal point vs incident 532-nm pulse energy for sample no. 3. The smaller slope (3.3±0.15) and larger indicated cross section [$\sigma^{(4)}=(2.75\pm1.0)\times10^{-112}$ cm^8 sec^3] compared with sample nos. 1 and 2 imply impurities may be playing a more important role in the absorption process.

The difference in interaction volumes (see Table I) does not explain the inconsistency in $\sigma^{(4)}_{\max}$ obtained from samples 1 and 3, since those of samples 1 and 2 were even more different but yielded consistent results. We thus attribute the discrepancy of $\sigma^{(4)}_{\max}$ in crystal 3 compared to samples 1 and 2 to the fact that they originate from different boules and, thus, from different starting material. Just like Manenkov,[33] we put our trust in the data of samples 1 and 2 because they exhibited higher threshold and agree well. Of the samples from the two boules, we believe the data from the first most nearly exhibit intrinsic (to pure NaCl) phenomena.

The uncertainties reported in Table I are the results of a mean-square error analysis of Eq. (8). Measurement error in the pulse energy, E ($\approx10\%$), and the beam waist, w_0 ($\approx5\%$), make the largest contributions to the uncertainty of $\sigma^{(4)}$. The temperatures in Figs. 3 and 4 have uncertainties of approximately 20%, with the most significant error being in the measurement of w_0.

In Ref. 7 we showed that the data obtained from measurement of prebreakdown energy deposition is inconsistent with the expectations derived from a simplified theory of self-focusing. Smith *et al.*[6,32] performed a series of measurements designed to obtain the breakdown threshold and critical power for self-focusing by measuring the energy of damaging pulses as a function of focal area, πw_0^2. The work presented by Manenkov,[33] and our experience, discussed above, indicates Smith *et al.* were probably not measuring intrinsic damage, since no special precautions regarding purity or sample selection were mentioned.

Our results[7] indicate that self-focusing is ineffective, at least up to the damage threshold. Since this work was completed it has come to our attention that Soileau *et al.*,[40] have shown that for tightly focused ($w_0<10$ μm) 532-nm pulses of subnanosecond duration in NaCl, self-focusing does not measurably occur for intensities up to the damage threshold. We therefore do not "correct" our results for self-focusing, but do list all the relevant parameters (Table I) so that it may be done, if desired.

IV. MODEL CALCULATIONS

A. Introduction

The total interaction between the laser photons and crystal is not merely multiphoton electron-hole (e-h) pair generation. Additionally, conduction-band electrons absorb energy from the photon field, as do certain so-called primary defects which are created as a result of e-h pair generation. For this reason, the four-photon absorption cross sections obtained from the data in the previous section are overestimated. Since we are only interested in *intrinsic* material we do not attempt to model effects due to impurities. But clearly, in light of experimental evidence discussed in Sec. III, such an investigation is warranted to explain the bulk of *extrinsic* laser damage data.

Complicating the picture is the fact that there are two theories of latitude heating resulting from the absorption of photons by electrons in the conduction band. The first is the polaron model, proposed by Schmid *et al.*,[3] in which the electrons are strongly coupled to the phonon system, and absorption of a single photon by an electron is followed by virtually instantaneous dissipation of the excess energy to the crystal lattice. In this model, an electron never absorbs more than one photon before relaxing back to the bottom of the conduction band. The second model is intimately connected with the avalanche theory of free-electron generation. The electron-phonon scattering necessary for energy extraction by free electrons from the electromagnetic field (required for electrons to attain sufficient energy for impact ionization) is the mechanism by which the lattice is heated. In both cases, phonons play the crucial role of the third particle necessary for the electron to absorb electromagnetic energy.

Highly accurate absorption parameters for the crystal excitations are not available, so that our modeling of the more complex laser-crystal interaction accounting for the presence of these species relies on the best estimates we could obtain. We show that the essential demonstration of the primary event of four-photon absorption; i.e., a fourth-order power-law relation for absorbed energy versus incident pulse energy, is not masked by free-carrier and defect absorption. For completeness we also consider the avalanche mechanism of e-h pair generation, both in the absence of four-photon carrier generation with an assumed starting density of conduction electrons, and four-photon assisted.

B. Electron-hole pair generation, primary defect production, and secondary energy absorption

The rate of increase of carriers in the conduction band due to four-photon absorption is given by Eq. (1) with $m=4$.

1. Avalanche generation and free-electron heating

In general, the avalanche mechanism results in a free-carrier generation rate of $dn_c/dt=\gamma n_c$, where γ is the avalanche coefficient, a complicated function of crystal properties, photon energy, and electric field strength. The form of the avalanche rate function γ depends to a large extent on the relation of the photon energy, $h\nu$, to the band gap energy E_g. For our experiments, $h\nu/E_g \approx 1/3.7$, so the case of $h\nu \ll E_g$, which pertains to the bulk of avalanche literature, is inappropriate for analysis here. A review of the American "low-frequency or small quanta" avalanche literature is given by Smith.[1] An extensive Soviet literature, largely due to Epifanov and co-workers,[5,41–44] also exists. These authors, and later, Sparks *et al.*,[45] derived an avalanche theory using a quantum diffusion analysis for the conduction electrons (in energy space) which removed some of the objections to the classical avalanche models reviewed by Smith. Only the Soviet group considered the case of avalanche in the presence of large quanta, $3 \le E_g/h\nu \le 5$, which requires modification of the diffusion avalanche theory to account for the large jump in energy an electron undergoes when it absorbs a photon of energy approximately 2 eV; i.e., a differential approximation for energy gain from the field is no longer valid.[42] This investigation was prompted by the disagreement of the damage threshold behavior with the small quanta theory in high threshold alkali halides (including NaCl) with four-photon band gaps at 532 nm.[5] It was speculated that the disagreement was at least partially due to four-photon e-h pair generation.

For the case of 532-nm photons interacting with conduction electrons in NaCl ($E_g=8.6$ eV), the avalanche coefficient γ is given by (using notation of Gorshkov *et al.*[42]) $\gamma=Q(1)\gamma_0$, where for a four-photon band gap $\gamma_0 \approx (4^6/4!)(q\delta)^5$, $Q(1)$ is the rate constant at which electrons lose energy by acoustical phonon scattering [$Q(1) \approx 5\times10^{13}$ sec^{-1} which is approximately one-tenth of the electron-phonon collision frequency, estimated to be approximately 6×10^{14} sec^{-1} in Refs. 5 and 45]. The dimensionless product $q\delta$ is given by $q\delta \approx a(T/T_0)E^2$, which arises from the solution of the diffusion equation. E is the electric field maximum amplitude, T is the lattice temperature, $T_0=300$ K, and a is a coefficient equal to $e^2kT_0/6m^2v_s^2(2\pi\nu)^2E_g \approx 5\times10^{-16}$ (cm/V)^2, where e and m are the charge and mass of the electron, k is Boltzmann's constant, and v_s is the longitudinal sound velocity. In terms of intensity, E^2 (in V^2/cm^2)$=240\pi I$(W/cm^2)n, where n is the index of refraction. In terms of flux, $F=I/h\nu$, this reduces to

$$\gamma \approx 5\times10^{13}\gamma_0 \text{ sec}^{-1}$$
$$\approx 1.5\times10^{-62}[a(T/T_0)F/n]^5 \text{ (sec}^{-1}) , \quad (10)$$

and

$$3\times10^{-17} \le a \le 1\times10^{-15} \text{ (in units of cm}^2/\text{V}^2)$$

for NaCl. The large range for a in NaCl arises from uncertainties in the effective mass of electrons and collision frequencies, and leads to an enormous uncertainty in γ, demonstrating the difficulties encountered in modeling the interaction of laser photons with wide gap materials.

Lattice heating due to the electron-phonon scattering implicit in the avalanche generation of free carriers can be reduced to the form

$$\rho c(dT/dt) \approx (mkT/2\pi)^{1/2}(eE/2m\pi\nu)^3 n_c/l_{ac}v_s ,$$

where l_{ac} is the mean free path of an electron between collisions with acoustic phonons. Again we have a rather wide latitude in this heating term due to uncertainties in the effective mass of the carriers, m, and the mean free path l_{ac}. Since both of these parameters are functions of the electron energy, some intermediate value must be assumed. The effective mass of a low-energy carrier may be as low as $0.5m_e$ (m_e is the free electron mass).[46] We assume a value of $m \approx 0.75m_e$. The electron mean free path is estimated by $l_{ac} \sim v\tau_{coll}$, where v is the electron velocity ($v=\sqrt{2\epsilon/m}$) and τ_{coll} is the reciprocal collision frequency. The average energy of the free carriers under predamage conditions is probably considerably less than $E_g/2$ (approximately 4.3 eV for NaCl). We assume $\epsilon \approx 2$ eV and $\tau_{coll} \sim 1/(6\times10^{14}$ sec$^{-1})$ and obtain $l_{ac} \sim 10^{-7}$ cm. With these values the lattice heating relation is

$$\rho c(dT/dt) \approx 8.3\times10^{-29}E^3T^{1/2}n_c \text{ (J/cm}^3 \text{ sec)} , \quad (11)$$

where E is in V/cm. Of course, this value is highly uncertain; the nature of the uncertainties will be discussed below in relation to the calculated results.

For computation of heating with an avalanche-only carrier generation mechanism, a number of electrons must be initially present in the conduction band, supposedly arising from shallow electron traps imposed by impurities. In the literature, it is commonly held that the avalanche builds from initial carrier density of 10^{11}–10^{13} cm^{-3},[43] but due to the rapid carrier buildup once the avalanche rate γ gets large during a laser pulse, the calculations are not very sensitive to variations in this parameter.

2. Polaron heating

The case where free carriers are considered to be polarons is discussed in detail in Ref. 3. The single photon absorption cross section for polarons in NaCl is $\sigma_p \approx 5.5\times10^{-19}$ cm^2 at 532 nm, for temperatures from 300 to 600 K. This value is obtained from the acoustic phonon scattering mechanism,[47] which has been shown to be the most effective when free-carrier velocities are not "slow."[3,41–45]

3. Primary defects

The responses of alkali halides following electron-hole pair creation, and their possible relation to laser-induced

damage, has been discussed in Refs. 48 and 14. The rate equations in these works were derived primarily for the purpose of calculating the effects of primary defect absorption on self-trapped exciton (STE) luminescence yield. Here we particularize the model equations to NaCl for our experimental conditions. Our goal is to model energy deposition and lattice heating at high temperatures (where STE luminescence is quenched), and production of permanent defects (F centers).

The processes modeled by the rate equations in Table II are depicted in Fig. 4. The details are available in Ref. 29. Free holes are trapped in a time of order 10^{-13} sec,[49] forming a V_K center along one of the six equivalent $\langle 110 \rangle$ crystal lattice directions with equal probability one-sixth. The V_K center has a cross section for capture of free carriers in the conduction band of $\sigma \approx 4\times 10^{-14}$ cm^2,[29,49] resulting in the formation of self-trapped excitons (STE's) or direct, nonradiative electron-hole recombination. A fraction $\gamma_1 = 0.025$ of captured electrons occupy the singlet (σ-luminescent) STE state, S_1, $\gamma_3 = 0.19$ form the triplet (π-luminescent) state, S_3, and $\gamma_0 = 0.785$ nonradiatively recombine with the trapped hole directly.[29] However, at high temperature the STE's decay nonradiatively; their importance in the model arises from the fact that they may be excited or ionized, and S_3 decays to F-H pairs on a time scale of 815 psec at 300 K.[50] The state S^* is that reached by absorption of a 2.33 eV photon by an S_3 STE. S^* decays to S_3 and S_1 excitons and F centers in the proportions $S_3{:}S_1{:}F = 0.97{:}0.027{:}0.003$,[51,52] if it is not ionized.

TABLE II. Model equations.

$$dn_c/dt = A^* - \sigma n_c v V_K + \sigma_h (S_1 + S^*)F + \sigma_{S^*} S^* F + \sigma_{S1} S_1 F + \sigma_F n_F F - \beta n_F^+ n_c$$

$$dp/dt = A^* - p/\tau_{VK} + 4\sigma_h V_{K1} F + \sigma_h V_{K2} F + (0) V_{K3} F$$

$$dV_{K1}/dt = \tfrac{1}{6} p/\tau_{VK} - \gamma_0 \sigma n_c v V_{K1} + (\tfrac{1}{6})(\sigma_h + \sigma_{S^*}) S^* F + \tfrac{1}{6}(\sigma_h + \sigma_{S1}) S_1 F - 4\sigma_h V_{K1} F$$

$$dV_{K2}/dt = \tfrac{4}{6} p/\tau_{VK} - \gamma_0 \sigma n_c v V_{K2} + (\tfrac{4}{6})(\sigma_h + \sigma_{S^*}) S^* F + \tfrac{4}{6}(\sigma_h + \sigma_{S1}) S_1 F - \sigma_h V_{K2} F$$

$$dV_{K3}/dt = \tfrac{1}{6} p/\tau_{VK} - \gamma_0 \sigma n_c v V_{K3} + \tfrac{1}{6}(\sigma_h + \sigma_{S^*}) S^* F + \tfrac{1}{6}(\sigma_h + \sigma_{S1}) S_1 F - (0) V_{K3} F$$

$$V_K = V_{K1} + V_{K2} + V_{K3}$$

$$dS^*/dt = (\sigma_h + \sigma_{S3}) S_3 F - (\sigma_h + \sigma_{S^*}) S^* F - S^*/\tau_{S^*}$$

$$dS_1/dt = \gamma_1 \sigma v n_c V_K - (\sigma_h + \sigma_{S1}) S_1 F + \eta_1 S^*/\tau_{S^*} - S_1/\tau_{S1}$$

$$dS_3/dt = \gamma_3 \sigma v n_c V_K - (\sigma_h + \sigma_{S3}) S_3 F + \eta_3 S^*/\tau_{S^*} - S_3/\tau_F$$

$$dn_F/dt = S_3/\tau_F + n_c \beta n_F^+ + \eta_F S^*/\tau_{S^*} - \sigma_F n_F F$$

$$dn_F^+/dt = \sigma_F n_F F - n_c \beta n_F^+$$

$$\rho c dT/dt = B^* + \sigma n_c v V_K [\gamma_0 (E_g - E_{VK}) + \gamma_1 E_{S1} + \gamma_3 E_{S3}] + (p/\tau_{VK}) E_{VK} + (\sigma_h + \sigma_{S^*}) S^* F (h\nu - E_{S^*}) + (\sigma_h + \sigma_{S1}) S_1 F (h\nu - E_{S1}) + \eta_3 (S^*/\tau_{S^*}) h\nu + \eta_1 (S^*/\tau_{S^*})(E_{S1} - E_{S^*}) + \eta_F (S^*/\tau_{S^*}) h\nu + (S_1/\tau_{S1})(E_g - E_{S1} - E_{VK}) + \beta n_c n_F^+ E_F$$

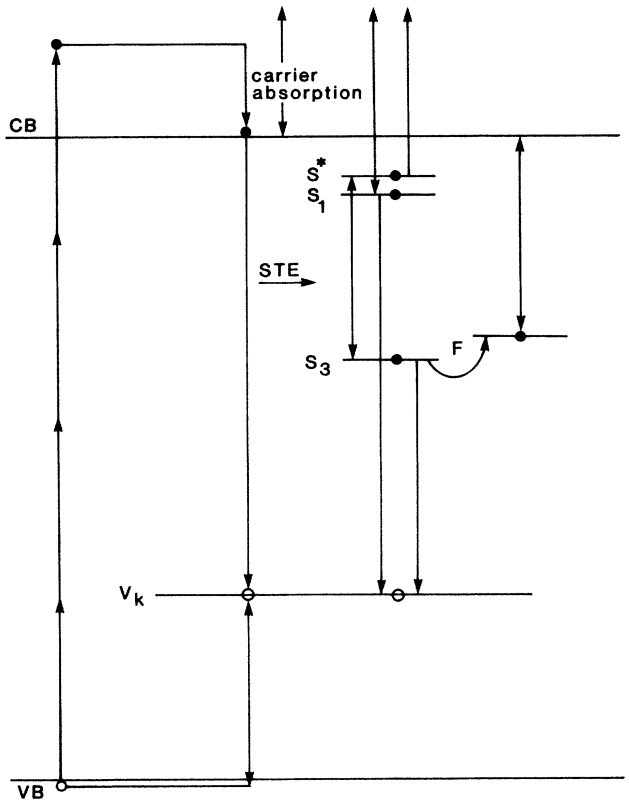

FIG. 4. Level diagram and transitions incorporated in model equations. Four-photon-generated free carriers and holes are trapped to form STE's and V_K centers. Holes can be released by single photon absorption, as can electrons in the S_1 and S^* STE states. Electrons in S_3 can be excited to S^* by single photon absorption. All downward electron transitions are nonradiative in model calculations. Free carriers can also absorb electromagnetic energy. At high temperature, F centers are formed through the S_3 STE state.

Self-trapped hole absorption (henceforth simply hole absorption) and V_K center orientation are important aspects of the model calculations.[29,14] The hole level is placed at 2.33 eV above the valence band since the net effect of a hole absorbing a laser photon is dissipation of this energy.

The primary defect contributions to lattice heating arise from the energy dissipated as a result of their formation and their photon absorption characteristics. These are listed in Table III. The absorption cross sections are obtained from measured absorption spectra with assumed values for the oscillator strength for use in Smakula's equation. The assumed oscillator strength is 0.78, equal to that of the F center.[53] Absolute cross sections for other absorbing species are not known. Single photon absorption cross sections for S_1 and S^* STE's

are assumed to be of the order 5×10^{-17} cm^2, reasonable for transitions into a continuum. More accurate values are not important because the photon flux is so high.

In order to extrapolate the low-temperature data for the calculation of photon absorption cross sections to 300 K, we work with the assumption that the same basic processes are in effect but that lifetimes are much shorter in general and nonradiative processes replace radiative ones. The only real room-temperature data are the STE to F conversion, and F-center properties. The kinetic equations are presented together with explanations summarizing this discussion in Tables II and III.

4. *Diffusion of defects and free carriers*

The diffusion of V_K centers and STE's in NaCl was discussed by Tanimura and Itoh.[54] From this work we conclude that for temperatures up to at least 600 K, the diffusion length for V_K centers and STE's is approxi-

TABLE III. Definition and value of parameters in model equations.

n_c	Conduction-band carrier concentration, polarons or free electrons
p	Free-hole density
V_{K1}	Density of V_K centers parallel to [110] laser polarization
V_{K2}	Density of V_K centers at angle to [110]
V_{K3}	Density of V_K centers oriented perpendicular to [110]
S_1	Density of STE's in singlet state S_1
S_3	Density of STE's in triplet state S_3
S^*	Density STE's in higher excited state (S^*)
n_F	F-center density
n_F^+	Ionized F-center density
$N=2.23\times10^{22}$ cm^{-3}	Density of active atoms (i.e., Cl^- ions)
F	Photon flux in photons/cm^2 sec
$\tau_{V_K}\approx10^{-13}$ sec	Formation time of V_K center or free-hole lifetime[a]
$\tau_{S1}=8\times10^{-12}$ sec	Nonradiative lifetime of S_1 STE[b]
$\tau_F=815\times10^{-12}$ sec	Nonradiative lifetime of $S_3\rightarrow F$-center conversion[c]
$\tau_{S^*}=5\times10^{-12}$ sec	Nonradiative lifetime of S^* STE
$\sigma=4\times10^{-14}$ cm^2	Cross section for capture of free carrier by V_K[a]
$\sigma_h=8.6\times10^{-18}$ cm^2	Single photon absorption cross section for trapped holes at 532 nm[d]
$\sigma_{S^*}=5\times10^{-17}$ cm^2	Absorption cross section for S^* STE at 532 nm[e]
$\sigma_{S1}=5\times10^{-17}$ cm^2	Absorption cross section for S_1 STE at 532 nm[e]
$\sigma_{S3}=1.2\times10^{-16}$ cm^2	Absorption cross section for S_3 STE at 532 nm[d]
$\sigma_F=5\times10^{-17}$ cm^2	Absorption cross section for F center at 532 nm[f]
$\beta=1.45\times10^{-6}$ cm^3/sec	Probability for ionized F center to capture free carrier[g]
$\gamma_0=0.785$	Branching fraction for direct recombination of e-h
$\gamma_1=0.025$	Branching fraction for S_1 STE formation[h]
$\gamma_3=0.19$	Branching fraction for S_3 STE formation[a]
$\eta_1=0.027$	Branching fraction of $S^*\rightarrow S_1$[i]
$\eta_3=0.97$	Branching fraction of $S^*\rightarrow S_3$[i]
$\eta_F=0.003$	Branching fraction of $S^*\rightarrow F$ center[i]
$v\approx10^7$ cm/sec	Free-carrier velocity[e]
$E_g=8.6$ eV	Energy gap of NaCl
$E_{S1}=0.9$ eV	Depth of S_1 state below conduction band[e]
$E_{S3}=2.9$ eV	Depth of S_3 state below conduction band[h]
$E_{S^*}=0.6$ eV	Depth of S^* state below conduction band[e]
$E_{VK}=2.33$ eV	Energy given to lattice when V_K bond forms[e]
$E_F=2.76$ eV	Depth of F center below conduction band[f]
$h\nu=2.33$ eV	Photon energy at 532 nm
$\sigma_p\approx5.5\times10^{-19}$ cm^2	Polaron absorption cross section at 532 nm[j]
$A^*=\sigma^{(4)}NF^4$	In multiphoton-polaron model
$A^*=\sigma^{(4)}NF^4+\gamma n_c$	In multiphoton-assisted avalanche model, where γ is given by Eq. (10)
$A^*=\gamma=n_c$	In avalanche-only model
$B^*=\sigma^{(4)}NF^4\ (4h\nu-E_g)$ $+\sigma_p n_c F h\nu$	In multiphoton-polaron model In multiphoton-free electron heating, multiphoton assisted avalanche, and avalanche-only models, B^* is given by Eq. (11)

[a]Reference 49.
[b]Reference 55.
[c]Reference 50.
[d]References 56 and 57.
[e]Reference 29.
[f]Reference 53.
[g]Reference 2.
[h]Reference 58.
[i]References 51 and 52.
[j]References 3 and 47.

mately 3 orders of magnitude smaller than a spot radius of ~ 5 μm for a pulse duration of order 100 psec.

Free-electron diffusion was considered in terms of laser damage by Epifanov.[43] He derived a condition on the laser focal spot radius which delineates the importance of carrier diffusion. If the laser spot radius is much greater than a critical radius, diffusion can be neglected. For 3-nsec pulses and a mean free path between acoustic phonon collisions of $l_{ac} \sim 10^{-6}$ cm, he obtained a critical radius of approximately 10 μm. For subthreshold pulses, we can assume the average kinetic energy of the carriers to be lower, and for pulse lengths of $\tau \approx 85$ psec, we expect a critical radius smaller by at least a factor equal to the square root of the ratio of assumed pulse lengths, or a critical radius of less than approximately 2 μm, smaller than any spot radius used in our experiments.

Neglecting thermal diffusion as well as that of defects and free carriers, we can calculate the temperature increase at the focal point of the laser beam in the model by considering only the photon flux at the focal point.

C. Model equations

We calculate the focal point temperature increase, ΔT_0, versus peak laser flux, F_p, for essentially three different models. These are

(1) Multiphoton-polaron-defect heating.
(2) Multiphoton-assisted avalanche heating.
(3) Unassisted avalanche heating.

Model (1) has a variation wherein we exchange free electron and polaron heating terms. In model (2), multiphoton free-carrier generation provides starting electrons for the avalanche, and in model (3) we assume a starting electron density n_{co}.

We have derived a set of coupled differential equations for the concentrations of the various species and the rise in lattice temperature. The terms in the temperature equation are self-explanatory when Table III is consulted. In addition to those defects already discussed, we include the probability, β, for free electrons capture by ionized F centers (or Cl^- vacancies) denoted as F^+ centers.[2] Free holes, p, are created when electrons are excited from the valence band and also when a V_K center is dissociated by hole absorption. The energy dissipated in the lattice by hole trapping appears as $(p/\tau_{V_K})E_{V_K}$.

For computational convenience, the laser pulse was expressed as $F(t)=F_p \exp(-[(t/\tau)-\sqrt{5}]^2)$; the calculation begins at $t=0$, and the pulse peaks at $t=190$ psec for $\tau=85$ psec. The equations, listed in Table II, were solved using the Runge-Kutta method.

D. Modeling results

1. *Principal findings*

Our aim was to computer simulate the intrinsic behavior of NaCl, that is, to reproduce the experimental results shown in Fig. 2 by varying $\sigma^{(4)}$ in the various models described above. We achieved this only for models

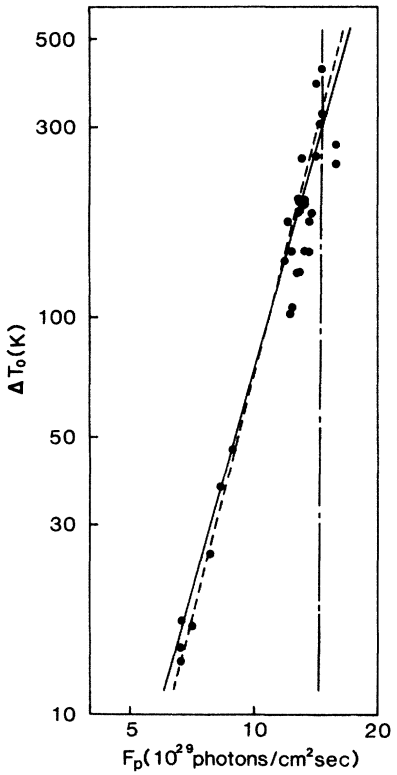

FIG. 5. Model calculations superimposed on data of sample nos. 1 and 2 (Fig. 2). The solid line is that calculated with the four-photon-polaron model, using $\sigma^{(4)}=2\times10^{-113}$ cm^8 sec^3; the slope is ≈ 3.7. The dashed line is that obtained with the four-photon-free electron model, using $\sigma^{(4)}=1.5\times10^{-114}$ cm^8 sec^3; the slope is 3.93. The broken line was obtained with the avalanche-free electron model, using $a=3\times10^{-16}$ and initial carrier density $n_{co}\approx 7\times10^{10}$ cm^{-3}.

where four-photon absorption was the sole mechanism for e-h pair generation (see Fig. 5). Due to the approximate nature of most model parameters, a "best fit" was not sought in the calculations, but rather a reasonable one satisfactorily accounting for the data. Implicit in the principal results are the defect concentrations and the individual contributions to the temperature increase, obtained from the model equations. The results for each model are summarized as follows.

1(a). Multiphoton-polaron-defect model. The approximation to the data for this model is represented by the solid line in Fig. 5, obtained with $\sigma^{(4)}=2\times10^{-113}$ cm^8 sec^3. This indicates that (in this model) direct e-h recombination contributes significantly to the heating, since this value of $\sigma^{(4)}$ is quite close to that obtained experimentally by assuming all heating arises from recombination ($\sigma^{(4)}\approx 5\times10^{-113}$ cm^8 sec^3). The slope of the solid line is approximately 3.7, showing that, even though other mechanisms contribute to the heating, four-photon absorption is the primary interaction of the overall process and that a photoacoustic demonstration of four-photon absorption is valid. In this model, only hole absorption, direct e-h recombination, and polaron absorption contribute to heating, with other species contributing much less. We consider this in more detail below.

1(b). Multiphoton free-electron-defect model. When the free-electron heating expression is substituted for the polaron heating term, we obtain the dashed line in Fig. 5 with $\sigma^{(4)} \approx 1.5 \times 10^{-114}$ cm^8 sec^3 to yield a reasonable fit. The slope of this line is 3.93, again indicating four-photon absorption is the primary process of the overall interaction, although clearly in this case direct e-h recombination plays a minor role in heating and the free-electron heating mechanism is much more efficient than polaron heating. This is reflected by the much smaller value of $\sigma^{(4)}$ needed to approximate the data, which implies fewer conduction-band carriers are needed to heat the sample.

2. Multiphoton-assisted avalanche with free-electron heating model. No value of the parameter a [see Eq. (10)] in the range $3 \times 10^{-17} \leq a \leq 1 \times 10^{-15}$ could account for the experimental data. Either a had to be so small that avalanche multiplication was negligible or, if a was large enough to contribute at all, it was explosive as the nearly vertical line in Fig. 5 indicates for the avalanche only mechanism.

3. Avalanche e-h generation—free-electron heating model. The model with avalanche carrier generation as the only mechanism for valence electron excitation is represented by the broken, nearly vertical line in Fig. 5, with $a = 3 \times 10^{-16}$ and a starting carrier density of $n_{co} \approx 7 \times 10^{10}$ cm^{-3}, chosen to match the highest temperature point. This line demonstrates the general behavior of the avalanche model. Varying a only displaces the line horizontally (to lower flux for larger a and vice versa). Slightly less steep lines may be obtained for a near the low end of its range but only for $n_{co} \geq 10^{17}$ cm^{-3}, for which the crystal would no longer be transparent anyway. Thus we conclude that the avalanche mechanism (as we have used it) plays no role in carrier generation up to the temperatures we have obtained. However, it is clear that it would be nearly impossible to measure predamage energy deposition if it were due to avalanche generation. Since temperatures we measured do not reach the melting point (a damage criterion), we cannot conclude with certainty that avalanche formation does not occur or play a role in laser damage.

It is clear why the avalanche mechanism is often invoked to explain the threshold aspect of extrinsic laser damage. The line in Fig. 5 representing the avalanche model demonstrates the perceived aspect of negligible absorption below threshold and explosive heating at or above threshold.

2. *Detailed model results*

Here we present the details of the temperature increase at a typical point in the data set, $\Delta T_0 \cong 217\,^\circ$C and $F_p = 1.34 \times 10^{30}$ photons/cm^2 sec, for both the polaron and free-electron heating models with four-photon e-h pair generation.

In the polaron-defect model [model 1(a)], heating is dominated by hole absorption, followed by direct e-h recombination and finally polaron absorption, and in the free-electron-defect model, heating is completely dominated by the free-electron heating term.

We summarize the results in the following paragraphs and figures. We shall refer to model 1(a) as the polaron model and 1(b) as the free-electron model. The four-photon cross section used were $\sigma^{(4)} = 2 \times 10^{-113}$ cm^8 sec^3 in model 1(a) and $\sigma^{(4)} = 1.5 \times 10^{-114}$ cm^8 sec^3 in model 1(b). The temperatures are expressed in Kelvin and the starting temperature is 293 K. A tabular summary of the computational results is presented in Table IV, where the peak concentrations of each species is given for each model, as well as the major contributions to the temperature increase.

In Fig. 6 the solid curve represents the total temperature increase in the polaron model and the dashed curve the free-electron model. The total increase is 215 K and 218 K, respectively, achieved with a pulse of peak flux of $F_p = 1.3 \times 10^{30}$ photons/cm^2 sec. These temperatures do not agree exactly for we have not tried to obtain precise results due to the inexact nature of the model parameters. There is only slight variation in the heating rate for the two models.

Polaron and hole absorption and e-h recombination account for approximately 208 K of the 215 K total temperature increase in the polaron model. Ignored in the recombination is the 0.7 eV difference between the e-h pair creation energy ($4h\nu = 9.3$ eV) and the band gap of 8.6 eV, which the electrons dissipate while relaxing to the bottom of the conduction band. This term accounts for most of the difference between the total temperature increase and that of the three dominant terms.

The free-electron contribution to the total temperature increase in model 1(b) is 204 K of the total rise of 218 K. Clearly, as we have used it, the free-electron model predicts very efficient heating of the lattice through electron-phonon scattering. The carrier and defect densities calculated in this model are much smaller than in the polaron model, reflecting on the much smaller value of $\sigma^{(4)}$ in this model to account for the experimental data. The temperature deficit was mostly accounted for by hole absorption. The heating rate (first derivative of the curves in Fig. 6) peaks with the photon flux for both models, but the rate function is much narrower than the

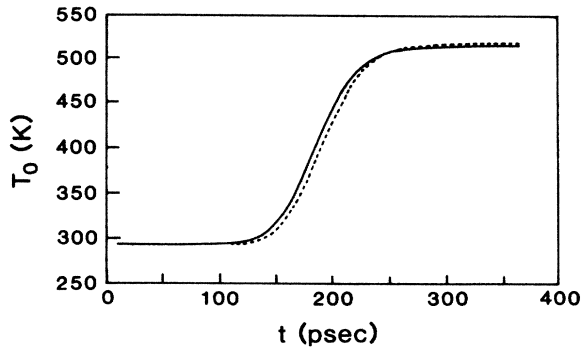

FIG. 6. Focal point temperature, T_0, vs time calculated for a pulse with $F_p = 1.34 \times 10^{30}$ photons/cm^2 sec. Solid line: multiphoton-polaron model [model 1(a)] using $\sigma^{(4)} = 2 \times 10^{-113}$ cm^8 sec^3. Dashed line: multiphoton-free electron model [model 1(b)], $\sigma^{(4)} = 1.5 \times 10^{-114}$ cm^8 sec^3. Laser pulse "begins" at $t = 0$, with flux $F = F_p \exp\{[(t/\tau) - \sqrt{5}]2\}$, $\tau = 85$ psec.

TABLE IV. Modeling results simulating the data point $F_p = 1.3\times10^{30}$ photons/cm^2 sec and $\Delta T_0 \approx 217$ K.

$\sigma^{(4)}$	Multiphoton-polaron 2×10^{-113} cm^8 sec^3	Multiphoton-free electron 1.5×10^{-114} cm^8 sec^3
Species	Peak concentrations (cm^{-3})	
n_c	3×10^{18}	8.5×10^{17}
p	8×10^{17}	7×10^{16}
V_{K1}	3×10^{16}	2.5×10^{15}
V_{K2}	4.5×10^{17}	4.5×10^{16}
V_{K3}	2.3×10^{18}	7.6×10^{17}
S_1	3.6×10^{14}	3.6×10^{13}
S_3	1.5×10^{15}	1.2×10^{14}
S^*	3.2×10^{15}	1.2×10^{14}
F	a	a
F^+	a	a
	Major heating contributions	
Free carriers	37 K (polarons)	204 K
e-h recombination at V_K centers ($V_{K1}+V_{K2}+V_{K3}$)	50 K	
Hole absorption and retrapping	121 K	10 K
All other contributions	7 K	4 K

[a]See text for discussion.

laser pulse, so that instantaneous conversion of electromagnetic to thermal energy implicit in the photoacoustic discussion are justified. A maximum of 3×10^{12} K/sec is calculated for the modeled pulse.

Figure 7 represents the conduction carrier densities, n_c, as functions of time for the polaron model (solid curve) and free-electron model (dashed curve). The maximum concentrations are $n_{cmax}\approx3\times10^{18}$ cm^{-3} and 8.5×10^{17} cm^{-3}, respectively. Since this laser pulse represents a nondamaging one, it is apparent that merely achieving a carrier density of $n_c\approx10^{18}$ cm^{-3} does not account for damage. The concentrations n_c and p decay only slightly slower than they rise due to the efficient trapping of holes and carriers in and by V_K centers.

The calculated concentrations of free holes, V_{K1}, V_{K2}, and V_{K3} centers, as well as S_1, S_3, and S^* STE's appear very similar to that of n_c in Fig. 7, with their peak concentrations listed in Table IV. The STE's contribute negligibly to heating in both models. The STE concentrations peak with the flux, but then they begin to increase slowly again as the laser pulse tapers off (about $t=350$ psec). This subsequent increase occurs because of the relaxation of carriers (at 350 psec there is still a carrier concentration of $n_c\approx2\times10^{17}$ cm^{-3}), but the laser flux is not yet small relative to the STE cross sections and significant ionization of STE's still occurs even though primary e-h pair generation is very small. Thus most STE electrons are still being kicked back into the conduction band and subsequently lost through the direct recombination channel. This is why STE's do not build up to levels near that of n_c. Of course, in the free-electron model, their concentrations are even smaller.

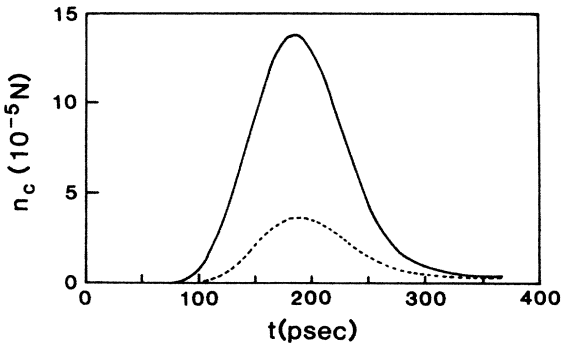

FIG. 7. Free-carrier density, in terms of the density of active atoms, $N=2.2\times10^{22}$ cm^{-3}. Many more carriers are generated in the polaron model (solid line) than in the free-electron model (dashed line).

Densities of both F centers and ionized F centers (n_F and n_F^+, respectively) are extremely small during the times of high flux, with n_F^+ decreasing (recapturing carriers) while n_F exhibits rapid increase at about the same time that the STE's begin their subsequent rise. At most, 19% of the carriers at 300 psec ($\approx2\times10^{17}$ cm^{-3}) will relax to the S_3 state (ignoring STE absorption), implying a maximum F-center concentration, due to $S_3\rightarrow F$ center conversion, of $n_F\approx4\times10^{16}$ cm^{-3} for $t\geq1$ nsec. However, following the detailed processes out to $t\approx1$ nsec (with the laser still "on," $F\cong5\times10^{-10}F_p$), we find that concentrations of new F centers do not exceed a few times 10^{15} cm^{-3}. All the above calculations were performed with n_F $(t=0)=0$. Using F-center starting concentrations [$n_F(0)$] equal to 10^{13} and 10^{15} cm^{-3}, we find no contribution to heating due to F centers. At $n_F(0)\approx10^{15}$ cm^{-3}, the crystal would be significantly colored, and we know this is not the case. Furthermore, about 80% of "new" F centers decay by F-H recombination on a microsecond time scale,[49,50] so that we can conclude that multiple-shot-on-one-site experiments

should not be influenced by F-center buildup (as far as absorbed energy is concerned).

In hindsight, the STE states contribute negligibly to energy absorption. Due to the complexity of the model(s) this could not be ascertained *a priori*. It is necessary to include them, however, to model F center buildup since they arise via decay of the S_3 STE state. The figure of approximately 80% direct recombination of e-h pairs, obtained from low-temperature data, is probably an underestimate for temperatures of 300 to 500 K, so the STE and F center concentrations we calculated probably are overestimates.

V. SUMMARY AND CONCLUSIONS

The photoacoustic technique used to obtain the experimental data clearly demonstrates the occurrence of fourth-order nonlinear absorption for nondamaging laser pulses, but does not yield an exact numerical value for the four-photon cross section $\sigma^{(4)}$, due to the nature of the photoacoustic response to total absorbed energy. The secondary absorption processes by free carriers and primary lattice defects have been shown to contribute significantly to energy absorption and subsequent material heating, but uncertainties in the requisite parameters preclude a definitive statement of their individual importance.

We believe that the temperature increases calculated from the calibrated absorbed energy data definitely prove that significant lattice heating occurs for nondamaging laser pulses without formation of an electron avalanche. As we have documented, the damage mechanism active in NaCl at 532 nm has not been unequivocally assigned to be either avalanche or multiphoton based on damage threshold measurements. This experimental verification of significant energy deposition due primarily to four-photon absorption is the most important result of this work. However, it does not prove one mechanism or the other is responsible for laser induced damage in NaCl at this wavelength, for we could not obtain data for which the calculated temperature increase was very near the melting point of 800 °C.

From our experience it is clear that further theoretical investigations should rely on data obtained only from the purest sample material available to test damage models. Use of inferior materials will only introduce more confusion than already exists in the field.

We feel that we have used reasonable values in the model calculations and that further calculation would prove nothing more in particular, for we have shown that four-photon absorption is the primary mechanism responsible for the experimental results. Naive interpretation of the data, ignoring secondary absorption, yields an overestimate of the four-photon absorption cross section $\sigma^{(4)}$, although we cannot say by how much. But we conclude, based on our interpretation of the experimental results, that the four-photon cross section must lie in the range 1×10^{-114} cm^8 sec^3 $\leq\sigma^{(4)}\leq 20\times10^{-114}$ cm^8 sec^3.

Deciding whether the polaron or free-electron heating model is more appropriate must be the subject of further experimentation. The predicted large contribution of hole absorption to heating in the polaron model could provide a means for verification of the polaron-defect model. For example, polarization dependence of the photoacoustic signal could be measured, but this would have to be performed at low temperature in a material with high luminescent efficiency (approaching unit efficiency) of e-h recombination, to provide an independent measure of carrier generation. Potassium iodide (KI) might prove to be the ideal material for such a study, since it has near unit luminescence efficiency[59,60] at liquid nitrogen temperature, which could easily be attained with the bulky acoustic apparatus. Circularly polarized light could be used to prevent the dichroic bleaching of V_K centers which would result in larger acoustic signal (i.e., energy absorption) than for linearly polarized light, if the polaron-defect model of secondary absorption is correct. In addition, if one were to repeat the photoacoustic measurement in a material for which a reliable, independently measured value of $\sigma^{(4)}$ were available, such as that of Shen *et al.* in KBr,[14] then the results of modeling the photoacoustic data would be less ambiguous. It could then possibly be decided which treatment of conduction-band carrier heating is correct. Recent experiments in KBr at 532 nm (four-photon band gap) support the free-electron mechanism as the correct one (in this material).[61] This indicates that $\sigma^{(4)}$ in NaCl is most likely near the lower end of the reported range. However, a complete study of a properly chosen alkali halide, using both the photoacoustic method to detect heat generation and the luminescence technique to measure free-carrier generation in the same material, preferably simultaneously, is warranted to elucidate exactly the importance of free carrier and defect absorption to energy deposition. Results can be (at least partially) carried over to the study of the more important materials of high-power laser components such as CaF_2, which have band gaps and defect properties similar to the alkali halides.

ACKNOWLEDGMENTS

We would like to thank Mr. Tom Casper and Mr. Xiao-An Shen for valuable assistance in the laboratory and Dr. Jeff Young for helpful suggestions. This work was supported by the National Science Foundation under Grant No. DMR-81-07099.

---

*Present address: Carl Schenk A.G., Landwehrstrasse 55, D-6100 Darmstadt, West Germany.

[1]W. L. Smith, Opt. Eng. **17**, 489 (1978).

[2]P. Braunlich, A. Schmid, and P. Kelly, Appl. Phys. Lett. **26**, 150 (1975).

[3]A. Schmid, P. Braunlich, and P. Kelly, Phys. Rev. B **16**, 4569 (1977).

[4]P. Kelly, A. Schmid, and P. Braunlich, Phys. Rev. B **20**, 815

(1979).
[5]B. G. Gorshkov, Yu. K. Danileiko, A. S. Epifanov, V. A. Lobachev, A. A. Manenkov, and A. V. Sidorin, Zh. Eksp. Teor. Fiz. **72**, 1171 (1979) [Sov. Phys.—JETP **45**, 612 (1977)].
[6]W. L. Smith, J. H. Bechtel, and N. Bloembergen, Phys. Rev. B **15**, 4039 (1977).
[7]Scott C. Jones, X. A. Shen, P. F. Braunlich, Paul Kelly, and A. S. Epifanov, Phys. Rev. B **15**, 894 (1987).
[8]M. D. Levenson, *Introduction to Nonlinear Laser Spectroscopy* (Academic, New York, 1982).
[9]V. Nathan, A. H. Guenther, and S. S. Mitra, J. Opt. Soc. Am. B **2**, 294 (1985).
[10]V. S. Dneprovskii, D. N. Klyshko, and A. N. Penin, Pis'ma Zh. Eksp. Teor. Fiz. **3**, 385 (1966) [Sov. Phys.—JETP Lett. **3**, 251 (1966)].
[11]G. I. Aseev, M. L. Kats, and V. K. Nikol'skii, Pis'ma Zh. Eksp. Teor. Fiz. **8**, 174 (1968) [Sov. Phys.—JETP Lett. **8**, 103 (1968)].
[12]I. M. Catalano, A. Cingolani, and A. Minatra, Phys. Rev. B **5**, 1629 (1972).
[13]R. T. Williams, P. H. Klein, and C. L. Marquardt, in *Laser Induced Damage in Optical Materials*, Nat. Bur. Stand. (U.S.) Spec. Publ. No. 509, edited by A. J. Glass and A. H. Guenther (U.S. GPO, Washington, D.C., 1977), pp. 481–488.
[14]X. A. Shen, Scott C. Jones, Peter Braunlich, and Paul Kelly, Phys. Rev. B **36**, 2831 (1987).
[15]A. C. Tam and C. K. N. Patel, Nature **280**, 304 (1979).
[16]E. W. Van Stryland and M. A. Woodall, in *Laser Induced Damage in Optical Materials*, Nat. Bur. Stand. (U.S.) Spec. Publ. No. 620, edited by H. E. Bennett, A. J. Glass, A. H. Guenther, and B. E. Newnam (U.S. GPO, Washington, D.C., 1981), pp. 50–57.
[17]Q. Munir, E. Wintner, and A. J. Schmidt, Opt. Commun. **36**, 467 (1981).
[18]Y. Bae, J. J. Song, and Y. B. Kim, Appl. Opt. **21**, 35 (1982).
[19]Y. Bae, J. J. Song, and Y. B. Kim, J. Appl. Phys. **53**, 615 (1982).
[20]B. G. Gorshkov, L. M. Dorozhkin, A. S. Epifanov, A. A. Manenkov, and A. A. Panov, Zh. Eksp. Teor. Fiz. **88**, 21 (1985) [Sov. Phys.—JETP **61**, 12 (1985)].
[21]E. W. Van Stryland, M. A. Woodall, W. E. Williams, and M. J. Soileau, in *Laser Induced Damage in Optical Materials*, Nat. Bur. Stand. (U.S.) Spec. Publ. No. 638, edited by H. E. Bennett, A. H. Guenther, D. Milam, and B. E. Newnam (U.S. GPO, Washingtion, D.C., 1983), pp. 589–600.
[22]P. Horn, P. Braunlich, and A. Schmid, J. Opt. Soc. Am. B. **2**, 1095 (1985).
[23]P. Horn, A. Schmid, and P. Braunlich, IEEE J. Quantum Electron. **QE-19**, 1169 (1983).
[24]A. C. Tam, Rev. Mod. Phys. **58**, 381 (1986).
[25]C. K. N. Patel and A. C. Tam, Rev. Mod. Phys. **53**, 517 (1981).
[26]A. Rosencwaig and J. B. Willis, J. Appl. Phys. **51**, 4361 (1980).
[27]J.-M. Heritier, J. E. Fouqnet, and A. E. Siegman, Appl. Opt. **21**, 90 (1982).
[28]G. Liu, Appl. Opt. **21**, 955 (1982).
[29]Scott C. Jones, Ph. D. thesis, Washington State University, 1986.
[30]J. F. Nye, *Physcial Properties of Crystals* (Oxford University Press, New York, 1985).
[31]Amnon Yariv, *Quantum Electronics* (Wiley, New York, 1975).
[32]W. L. Smith, J. H. Bechtel, and N. Bloembergen, Phys. Rev. B **12**, 706 (1975).
[33]A. A. Manenkov, in *Laser Induced Damage in Optical Materials*, Nat. Bur. Stand. (U.S.) Spec. Publ. No. 509, edited by A. J. Glass and A. H. Guenther (U.S. GPO, Washington, D.C., 1977), pp. 455–464.
[34]Matthew Delong (private communication).
[35]H. W. Etzel and D. A. Patterson, Phys. Rev. **112**, 1112 (1958).
[36]J. Rolfe, Phys. Rev. Lett. **1**, 56 (1958).
[37]A dramatic verification of the first of these effects due to OH^- was obtained by exposing two wafers of ultrapure NaCl, one processed in the HCl atmosphere, to approximately 2 Mrad of γ radiation from a ^{60}Co source. The reactive atmosphere processed sample remained clear, while the unprocessed ultrapure sample turned amber in color (implying *F*-center creation) and, additionally, was riddled with black specks in the bulk, indicating agglomeration of defects.
[38]E. P. Ippen and C. V. Shank, in *Ultrashort Light Pulses; Picosecond Techniques and Their Applications*, edited by S. L. Shapiro (Springer-Verlag, Berlin, 1977).
[39]D. J. Bradley and G. H. C. New, Proc. IEEE **62**, 313 (1974).
[40]M. J. Soileau, W. E. Williams, and E. W. Van Stryland, in *Laser Induced Damage in Optical Materials*, Nat. Bur. Stand. (U.S.) Spec. Publ. No. 669, edited by A. H. Guenther, D. Milam and B. E. Newnam (U.S. GPO, Washington, D.C., 1984), pp. 387–405.
[41]A. S. Epifanov, A. A. Manenkov, and A. M. Prokhorov, Zh. Eksp. Teor. Fiz. **70**, 728 (1976) [Sov. Phys.—JETP **43**, 377 (1976)].
[42]B. G. Gorshkov, A. S. Epifanov, and A. A. Manenkov, Zh. Eksp. Teor. Fiz. **76**, 617 (1979) [Sov. Phys.—JETP **49**, 309 (1979)].
[43]A. S. Epifanov, Zh. Eksp. Teor. Fiz. **67**, 1805 (1974) [Sov. Phys.—JETP **40**, 897 (1975)].
[44]A. S. Epifanov, IEEE J. Quantum Electron. **QE-17**, 2018 (1981).
[45]M. Sparks, D. L. Mills, R. Warren, T. Holstein, A. A. Maradudin, L. J. Sham, E. Loh, and D. F. King, Phys. Rev. B **24**, 3519 (1981).
[46]J. T. Devreese, A. B. Kunz, and T. C. Collins, in *Polarons in Ionic Crystals and Polar Semiconductors*, edited by J. T. Devreese (North-Holland, Amsterdam, 1972).
[47]E. P. Pokatilov and V. M. Fomin, Phys. Status Solidi B **73**, 553 (1976).
[48]G. Brost, P. Braunlich, and P. Kelly, Phys. Rev. B **30**, 4675 (1984).
[49]R. T. Williams, J. N. Bradford, and W. L. Faust, Phys. Rev. B **18**, 7038 (1978).
[50]R. T. Williams, B. B. Craig, and W. L. Faust, Phys. Rev. Lett. **52**, 1709 (1984).
[51]K. Soda and N. Itoh, J. Phys. Soc. Jpn. **50**, 3988 (1981).
[52]K. Soda and N. Itoh, Phys. Lett. **73A**, 45 (1979).
[53]J. J. Markham, *F Centers in Alkali Halides* (Academic, New York, 1966), Suppl. 8.
[54]K. Tanimura and N. Itoh. J. Phys. Chem. Solids **42**, 901 (1981).
[55]S. Wakita, Y. Suzuki, H. Ohtami, S. Tagowa, and M. Hirai, J. Phys. Soc. Jpn. **50**, 3378 (1981).
[56]M. N. Kabler, in *General and Ionic Crystals*, Vol. 1 of *Point Defects in Solids*, edited by J. H. Crawford (Plenum, New York, 1972).
[57]R. T. Williams and M. N. Kabler, Phys. Rev. B **9**, 1897

(1974).
[58]M. Ikezawa and T. Kojima, J. Phys. Soc. Jpn. **27**, 1551 (1969).
[59]R. B. Murray and F. J. Keller, Phys. Rev. **137**, A942 (1965).
[60]K. J. Teegarden, Phys. Rev. **105**, 1222 (1957).
[61]X. A. Shen, Peter Braunlich, Scott C. Jones, and Paul Kelly, Phys. Rev. Lett. **59**, 1605 (1987).